J BONE ONCOL 49 (2024) 100652

Contents lists available at ScienceDirect

Journal of Bone Oncology

journal homepage: www.elsevier.com/locate/jbo

Research Paper

Novel lipid metabolism factor HIBCH inhibitor synergizes with doxorubicin to suppress osteosarcoma growth and impacts clinical prognosis in osteosarcoma patients

Xuhui Yuan [a,b,c,1], Bo Yu [d,1], Haiqi Ding [a,b,c], Hongyan Li [a,b,c], Qijing Wang [c,e], Lan Lin [a,b,c], Wenming Zhang [a,b,c,*], Xinyu Fang [a,b,c,*]

[a] Department of Orthopaedic Surgery, the First Affiliated Hospital, Fujian Medical University, Fuzhou 350005, China
[b] Department of Orthopaedic Surgery, National Regional Medical Center, Binhai Campus of the First Affiliated Hospital, Fujian Medical University, Fuzhou 350212, China
[c] Fujian Provincial Institute of Orthopedics, the First Affiliated Hospital, Fujian Medical University, Fuzhou 350005, China
[d] Department of Orthopedic, Huaqiao Hospital, Jinan University, Guangzhou, China
[e] Department of Orthopaedic, Affiliated Mindong of Fujian Medical University, Fuan, China

HIGHLIGHTS

- HlBCH promotes osteosarcoma malignancy by modulating TCA cycle metabolism.
- SBF-1 inhibitor suppresses tumor growth via Akt-mTOR pathway.
- Synergistic anti-tumor effects of SBF-1 and doxorubicin in vitro and in vivo.
- Novel therapeutic targeting strategy for osteosarcoma treatment.

ARTICLE INFO

Keywords:
Osteosarcoma
Lipid metabolism
HIBCH
TCA cycle
Akt-mTOR pathway
Synergistic effect

ABSTRACT

Background: Osteosarcoma (OS) is a highly malignant primary bone tumor primarily affecting children and adolescents. Despite advancements in therapeutic strategies, long-term survival rates for OS remain unfavorable, especially in advanced or recurrent cases. Emerging evidence has noted the involvement of lipid metabolism dysregulation in OS progression, but the specific mechanisms remain unclear.

Methods: A risk model incorporating lipid metabolism-related genes was established to stratify OS patients into high-risk and low-risk groups. Functional assays were conducted to assess the role of 3-hydroxyisobutyryl-CoA hydrolase (HIBCH) in OS cell activities. Ultra-fast liquid chromatography-mass spectrometry was adopted to analyze the impact of HIBCH on OS cell metabolism. Moreover, the combined effect of HIBCH inhibitor SBF-1 with doxorubicin (DOX) was evaluated through *in vitro* studies and mouse xenograft models.

Results: HIBCH was identified as a key gene involved in the malignant behaviors of OS cells. HIBCH knockdown disrupted tricarboxylic acid (TCA) cycle activity and reduced oxidative phosphorylation in OS cells. SBF-1 showed synergistic effects with DOX in inhibiting malignant phenotypes of OS cells by modulating the Akt-mTOR pathway. *In vivo* experiments demonstrated that the combination of SBF-1 and DOX significantly suppressed tumor growth in mouse xenograft models.

Conclusions: This study reveals the critical role of lipid metabolism in OS progression and suggests a new therapeutic strategy against chemotherapy resistance in OS based on the synergistic combination of SBF-1 with DOX.

* Corresponding authors at: Department of Orthopaedic Surgery, the First Affiliated Hospital, Fujian Medical University, Fuzhou 350005, China.
E-mail addresses: zhangwm0591@fjmu.edu.cn (W. Zhang), fangxinyu0417@fjmu.edu.cn (X. Fang).
[1] Xuhui Yuan and Bo Yu contributed equally to this work.

https://doi.org/10.1016/j.jbo.2024.100652
Received 29 August 2024; Received in revised form 4 November 2024; Accepted 18 November 2024
Available online 24 November 2024

1. Introduction

Osteosarcoma (OS) is the most common primary malignant bone tumor, which predominantly affects children and adolescents [1–3]. This malignancy typically arises in the long bones of the limbs, such as the femur, tibia, and humerus [1–4]. The primary symptom, pain, is often accompanied by other complications, such as swelling, limping, and overall health decline [3,4]. Despite advancements in multimodal treatment strategies, including surgery, chemotherapy (CT), and radiotherapy, the 5-year survival rates (5YSRs) for individuals with metastatic or recurrent OS remains alarmingly low at approximately 20–30 % [1,2,5]. The poor prognosis underscores the pressing need for novel therapeutic strategies and a deeper understanding of the molecular underpinnings of OS progression.

Recent investigations have increasingly highlighted the pivotal role of metabolic reprogramming in tumorigenesis and tumor growth [6,7]. Cancer cells exhibit notable metabolic adaptation, leading to rapid proliferation and survival in adverse conditions of tumor microenvironment [8]. Although conventional cancer research has focused on alterations in glucose metabolism, the functional relevance of lipid metabolism has gained increasing recognition in tumor biology [9,10]. Lipids, as essential structural components of cell membranes, play key roles in energy storage and signal transduction [11]. In the context of tumor development, alterations in lipid metabolism influence various malignant behaviors of cancer cells, such as proliferation, survival, migration, invasiveness, and metastasis [12,13]. These subtle yet significant metabolic modifications support the biological requirements of cancer cells and offer promising targets for the development of novel anti-cancer therapeutic strategies.

Lipid metabolism is implicated in complex pathways, including the synthesis, degradation, and regulation of fatty acids, phospholipids, and other lipid molecules. Dysregulation of these pathways has been associated with the carcinogenesis of various malignancies, such as breast, prostate, and colorectal cancers [14–16]. However, the specific role of lipid metabolism in OS remains to be fully elucidated. Emerging research has sought to unveil the potential functional implications of lipid metabolism in the pathophysiology of OS. In this context, Sun *et al.* have highlighted the overexpression of the lipid metabolism-related gene (LMRG) *YME1L* in OS, which fosters tumor growth through the regulation of lipid metabolism and the Akt-mTOR signaling pathway. Their findings underscore the potential of *YME1L* as a therapeutic target to impede OS progression [17]. Additionally, the LMRG *FAAH* has been identified as a potential biomarker for adverse outcomes in OS due to its capacity to enhance tumor growth and restrict apoptotic activities [18]. Furthermore, *ANGPTL4* downregulation has been demonstrated to disrupt branched-chain amino acid metabolism and activate the mTOR pathway in OS, leading to tumor progression [19].

Notably, 3-hydroxyisobutyryl-CoA hydrolase (HIBCH), a key enzyme in mitochondrial metabolism, is involved in the metabolic pathways of branched-chain amino acids and fatty acids [20]. Recent investigations have pinpointed *HIBCH* as a key gene in lipid metabolism and highlighted its significance in studies of tumor development. Alterations in HIBCH expression have shown notable associations with tumor progression and patient prognosis in clear cell renal cell carcinoma [21], suggesting its potential as a biomarker. Similarly, HIBCH plays a functional role in influencing tumor growth and invasive capabilities by modulating tumor cell metabolism in colorectal cancer [22]. Moreover, HIBCH expression may offer promising prognostic insights and serve as a therapeutic target in prostate cancer [23]. Despite these associations, the specific biological functions and mechanisms of HIBCH in OS have not been fully elucidated, indicating a pronounced gap in current research. This gap underscores the need for an in-depth investigation into the role of HIBCH in tumor metabolism and its potential as a therapeutic target.

This study aimed to clarify the role of lipid metabolism in OS development and its potential as a therapeutic target based on the analysis of LMRGs. The study focused on the functional relevance of HIBCH and examined its functions in malignant phenotypes of OS cells. Furthermore, the study integrated the lipid metabolism inhibitor with conventional CT to evaluate therapeutic effects and specifically examined the synergistic effects of HIBCH inhibitor with doxorubicin (DOX) in improving prognostic outcomes for OS patients. Therefore, this study highlighted the importance of lipid metabolism in modulating malignant phenotypes of OS and introduced a new perspective for enhancing therapeutic outcomes.

2. Materials and methods

2.1. Transcriptome data acquisition and preprocessing

Transcriptome data from 88 OS patients were acquired from the Therapeutically Applicable Research To Generate Effective Treatments (TARGET) database (https://ocg.cancer.gov/programs/target), with three samples excluded due to incomplete clinical records. Simultaneously, transcriptome data of 396 normal tissue samples, corresponding to the OS tissues, were retrieved from the Genotype-Tissue Expression (GTEx) database (https://www.gtexportal.org/home/). Data from TARGET and GTEx databases were normalized and logarithmically transformed ($\log_2(x+1)$) to enable efficient data integration and subsequent analysis. The merged data from TARGET and GTEx databases served as the training dataset. For validation, data from the GSE21257 Series Matrix File (annotated with platform GPL10295) were obtained from the National Center for Biotechnology Information (NCBI) Gene Expression Omnibus (GEO) database.

2.2. Identification and analysis of LMRGs

LMRGs were extracted from four gene sets in the Molecular Signatures Database (MSigDB) database, namely Reactome metabolism of lipids and lipoproteins, Reactome phospholipid metabolism, Hallmark fatty acid metabolism, and Kyoto Encyclopedia of Genes and Genomes (KEGG) glycerophospholipid metabolism. These genes were subsequently cross-referenced with the training and validation datasets to generate lipid metabolism-related expression matrices. Differential expression analysis was conducted utilizing the "*Limma*" package.

2.3. Construction and validation of a lipid metabolism-related prognostic risk model (RM)

The influence of lipid metabolism on prognostic survival was examined in OS patients based on the 176 candidate differentially expressed genes (DEGs) identified through differential expression analysis. A lipid metabolism-related prognostic RM was subsequently constructed and validated on training and validation datasets. Univariate Cox regression (UCR) analysis was initially performed to screen the candidate DEGs, resulting in six genes associated with prognosis. The prognostic model was constructed using the Least Absolute Shrinkage and Selection Operator (LASSO) regression. The risk score formula, shown below, was used to calculate the risk value for each OS patient:

$$\text{Risk score} = \sum_{i=1}^{n} Coef_i \times x_i$$

wherein $Coef_i$ represents the coefficient, and x_i denotes the gene expression value. Patients were stratified into the high-risk group (HRG) and the low-risk group (LRG) based on the median risk value, and survival curves were generated to compare prognostic outcomes between the two groups.

2.4. Cell culture, genetic modification, and treatment protocols

Human OS cell lines U2OS and U2R were obtained from the Cell

Bank of the Chinese Academy of Sciences (Shanghai, China). These cells were cultured in Dulbecco's Modified Eagle Medium (DMEM, Gibco, USA) supplemented with 10 % fetal bovine serum (FBS, Gibco) and 1 % penicillin–streptomycin (Gibco). All cultures were maintained at 37 °C in a 5 % CO_2-containing humidified incubator. Transfections for *HIBCH* gene interference and overexpression studies were performed using Lipofectamine 2000 (Invitrogen, USA) as the instructions described. *HIBCH*-targeting small interfering RNA (siRNA) was used for knockdown experiments, while overexpression was achieved with a plasmid encoding the full-length *HIBCH* gene. Transfection efficiency was examined 48 h post-transfection through RT-qPCR and Western blot analysis. To evaluate the synergistic effects of HIBCH inhibitor SBF-1 and DOX, U2OS and U2R cells were exposed to varying concentrations of these agents. The half-maximal inhibitory concentration (IC_{50}) values were calculated via the Cell Counting Kit-8 (CCK-8) assay, and the synergistic interactions were assessed using the Chou-Talalay method. Cells were treated with control (DMSO), single-agent (SBF-1 or DOX), or their combination for 48 h before subsequent analyses.

2.5. Cell viability, colony formation, transwell, and apoptosis assays

Cell viability was assessed using the CCK-8 assay (Dojindo Japan). U2OS and U2R cells were plated (2,000 cells per well) onto 96-well plates. For *HIBCH* knockdown and overexpression experiments, 10 μL of CCK-8 reagent was added to each well 48 h post-transfection, followed by incubation at 37 °C for 2 h. Then, absorbance was then measured at 450 nm using a microplate reader. For agent treatment studies, cells were exposed to SBF-1 and DOX for 48 h before the addition of CCK-8 reagent.

In the colony formation assay, U2OS and U2R cells were seeded (500 cells per well) into 6-well plates. For gene modulation experiments, cells were cultured for 10–14 days after transfection until visible colonies appeared. In agent treatment studies, cells were exposed to SBF-1 or DOX for 48 h and then allowed to grow for an additional 10–14 days. Colonies were fixed with 4 % paraformaldehyde, stained with crystal violet, and subsequently counted.

The migration and invasion of cells were examined using Transwell inserts (8 μm pore size; Corning, USA). For migration assays, U2OS or U2R cells (1×10^5) were suspended in a serum-free medium and placed in the upper insert, while the lower insert was filled with a medium containing 10 % FBS as a chemoattractant. For invasion assays, the upper inserts were pre-coated with Matrigel (BD Biosciences, USA). Following 48-h incubation, non-migratory and non-invasive cells were removed, while those that had migrated or invaded were fixed with 4 % paraformaldehyde, stained with crystal violet, and observed microscopically.

Cell apoptosis was assessed using the Annexin V-FITC/PI double staining method (BD Biosciences) and flow cytometry. U2OS and U2R cells were harvested 48 h after *HIBCH* gene modulation or agent treatment (SBF-1 or DOX) and stained according to the manufacturer's guidelines. Early and late apoptotic cell populations were analyzed using a BD FACSCanto II flow cytometer (USA). Each cellular experiment was performed in triplicate to ensure data reliability.

2.6. Real-time quantitative PCR (PCR)

Gene expression in OS cells was quantitatively assessed *via* real-time qPCR. Total RNA was extracted using TRIzol reagent (Invitrogen), and its concentration and purity were measured using a NanoDrop 2000 spectrophotometer (Thermo Scientific, USA). Subsequently, 1 μg RNA was reverse-transcribed into cDNA with the PrimeScript RT reagent kit (Takara, Japan). The qPCR reactions were carried out on an Applied Biosystems 7500 Real-Time PCR System using SYBR Green PCR Master Mix (Applied Biosystems, USA). Each reaction mixture contained 1 μL cDNA template, 10 μL SYBR Green Master Mix, 0.4 μL each of forward and reverse primers (10 μM), and 8.2 μL nuclease-free water. Thermal cycling conditions included an initial denaturation at 95 °C for 10 min, followed by 40 cycles of 95 °C for 15 s and 60 °C for 1 min. All samples were analyzed in triplicate. As normalized to GAPDH, relative gene expression was computed using the $2^{-\Delta\Delta Ct}$ method. The primer used are as follows:

HIBCH: 5′-GCAATTTCGAGTGGCTACAGA-3′ (forward) and 5′-CCTTGGAGTCGTGGCAAGAA-3′ (reverse).

GAPDH: 5′-GAAGGTGAAGGTCGGAGTC-3′ (forward) and 5′-GAAGATGGTGATGGGATTTC-3′ (reverse).

2.7. Metabolite extraction and metabolic analysis

Metabolomic analysis was performed on OS cells 72 h after *HIBCH* knockdown. Approximately 2.5×10^6 cells were harvested and subjected to three washes in ice-cold sterile PBS. Following centrifugation at 3000 rpm for 5 min, cell pellets were flash-frozen in liquid nitrogen and stored at −85 °C until further processing.

For metabolite extraction, 950 μL of a cold extraction mixture (methanol:water: chloroform = 7:2:1, v/v/v) was added to each cell sample. Cells were lysed by sonication on ice for 10 min, followed by centrifugation at 13,000*g* for 12 min at 4 °C to remove insoluble materials. From each sample, 850 μL of the supernatant was transferred to pre-chilled microcentrifuge tubes (1.5 mL), followed by the addition of 200 μL of a pre-cooled acetonitrile–water solution (4:1, v/v). Samples were subsequently dried under vacuum at 40 °C and reconstituted in 120 μL of chromatographic-grade acetonitrile–water solution (1:1, v/v).

The metabolomic analysis was conducted using UHPLC-Q-TOF/MS. Metabolites were separated on a Waters ACQUITY UPLC BEH Amide column (100 mm × 2.1 mm, 1.7 μm). The mobile phase included 10 mM ammonium formate in water with pH adjusted to 3.5 for phase A, and acetonitrile served as phase B. A 5 μL sample volume was injected, and the column temperature was maintained at 40 °C. Mass spectrometric data were collected in positive and negative ion modes, with a scan range of *m/z* 50–1000. MassLynx V4.1 software was employed for data acquisition and processing. Metabolite identification and relative quantification were determined by comparing accurate mass, MS/MS spectra, and retention times with reference standards. Metabolite peak areas were normalized against cell numbers, with tricarboxylic acid (TCA) cycle-related metabolites predominantly detected in the negative ion mode.

2.8. Measurement of NAD^+/NADH concentrations

NAD^+ and NADH concentrations were determined using the NAD^+/NADH Quantitation Colorimetric Kit (MAK037, Sigma-Aldrich) in accordance with the manufacturer's guidelines. Briefly, 1×10^6 cells were lysed in a specialized NADH/NAD extraction buffer. After centrifugation (14,000*g*, 5 min), the supernatant was extracted to quantify NAD^+ and NADH concentrations. The absorbance at 450 nm was recorded, and the corresponding concentrations were computed using a standard curve.

2.9. Western blot assay

The expression of HIBCH and associated proteins in OS cells was quantified through Western blot assay. U2OS and U2R cells were lysed in radio-immunoprecipitation assay (RIPA) buffer (Beyotime, China) containing a protease inhibitor cocktail (Roche, Switzerland). Protein concentrations were quantified using the bicinchoninic acid (BCA) kit (Pierce, USA). Protein samples (20–30 μg per lane) were separated by sodium dodecyl sulfate–polyacrylamide gel electrophoresis (SDS-PAGE; 10–12 %) and transferred onto polyvinylidene fluoride (PVDF) membranes (Millipore, USA). These membranes were blocked with 5 % skim milk for 1 h at ambient temperature, followed by overnight incubation with specific primary antibodies at 4 °C. Subsequently, membranes were subjected to incubation with horseradish peroxidase (HRP)-conjugated

secondary antibody (1:5000, Cell Signaling Technology, USA) for 1 h at ambient temperature. Protein bands were visualized using an enhanced chemiluminescence (ECL) substrate (Thermo Scientific), and the images were recorded using a ChemiDoc XRS+ imaging system (Bio-Rad, USA). Protein levels were semi-quantitatively analyzed using ImageJ software (NIH, USA), with normalization to β-actin (1:10000, Proteintech, Wuhan, China). The primary antibodies included HIBCH (1:1000) from Abcam (UK) and cleaved-PARP (1:1000), cleaved-caspase-9 (CASP-9) (1:1000), E-cadherin (1:1000), N-cadherin (1:1000), vimentin (1:1000), Akt (1:1000), mTOR (1:1000), p-Akt (1:1000), and p-mTOR (1:1000) from Cell Signaling Technology.

2.10. Cell transfection for HIBCH functional analysis

Cell transfection experiments were performed to explore the functional impacts of *HIBCH* on OS cells using plasmid-based gene overexpression in U2R cells and siRNA-mediated gene knockdown in U2OS cells. For *HIBCH* knockdown, siRNA targeting *HIBCH* (si*HIBCH*) and negative control siRNA (siNC) were purchased from GenePharma (China). For *HIBCH* overexpression, the plasmid harboring full-length *HIBCH* cDNA (pcDNA3.1-*HIBCH*) and the empty vector plasmid (pcDNA3.1) were obtained from GenePharma. U2OS or U2R cells, seeded in 6-well plates, were transfected at 60–70 % confluence using Lipofectamine 3000 reagent (Invitrogen). Knockdown and overexpression efficiencies were validated using qPCR and Western blot assays 48 h post-transfection.

Si-*HIBCH*-1: GCUCAUGUCGAGGUUUAAUTT
Si-*HIBCH*-2: GGUUACUUCCUUGCAUUAATT

2.11. Evaluation of synergistic effects of SBF-1 and DOX

The combination index (CI) was examined to evaluate the synergistic effects of SBF-1 and DOX on OS cell lines (U2OS and U2R). The cells, seeded in 96-well plates, were exposed to varying concentrations of SBF-1 and DOX alone or in combination for 48 h upon reaching approximately 70 % confluence. Cell viability was assessed using the CCK-8 assay (Dojindo), with 10 μL of CCK-8 reagent added to each well. The cells were incubated for 2 h at 37 °C. Absorbance was recorded at 450 nm using a microplate reader. CI values were calculated using the Chou-Talalay method and subsequently analyzed with CompuSyn software (ComboSyn, Inc., USA). CI values were critical for the assessment of drug interactions, where a CI < 1 indicated synergism, a CI $= 1$ suggested an additive effect, and a CI > 1 denoted antagonism. The results demonstrated notable synergistic cytotoxicity between SBF-1 and DOX in all tested OS cell lines, with CI values less than 1.

2.12. In vivo validation in a xenograft model

Animal experiments were conducted in strict accordance with the ARRIVE guidelines. A xenograft model was established using immunodeficient mice to further validate the anti-OS effects of the combined SBF-1 and DOX treatment *in vivo*. NOD-SCID mice (4–6 weeks old) were obtained from the Experimental Animal Center of The First Affiliated Hospital, Fujian Medical University. All animal experiments were approved by the Committee of The First Affiliated Hospital, Fujian Medical University and conducted in accordance with the *Guide for the Care and Use of Laboratory Animals*. Xenograft tumors were induced by subcutaneously injecting U2OS cells (1×10^7 cells suspended in 200 μL serum-free medium) into the right axillary region of the mice. Upon reaching tumor volumes of approximately 100 mm^3, the mice were randomly assigned into four groups (n = 6 per group): control (DMSO), SBF-1 alone (5 μg/kg), DOX alone (2 mg/kg), and combination treatment (SBF-1 5 μg/kg + DOX 2 mg/kg). Tumor volume and body weight were measured every 3 days during the treatment regimen. The formula used to calculate tumor volume was: volume = (length × $width^2$)/2. Agent administration was performed *via* tail vein injection every 3 days for 21 days. Upon completion of the experiment, the mice were euthanized, and tumor tissues were excised and weighed.

2.13. Statistical analysis

Statistical analyses were performed using GraphPad Prism 8.0 software. Each cellular experiment was replicated at least three times, with the results presented as mean ± standard deviation (SD). Differences between groups were compared using one-way analysis of variance (ANOVA) or Student's *t*-test. The Kaplan-Meier (KM) survival analysis with log-rank test was utilized to compare survival curves, and multivariate Cox regression (MCR) analysis was conducted using the Cox proportional hazards regression model. In *in vitro* and *in vivo* experiments, *post-hoc* tests with Bonferroni correction were used to address multiple comparisons. The level of significance was $p < 0.05$ (two-sided).

3. Results

3.1. Construction of a lipid metabolism-related RM for OS

The study begins with an examination of the LMRGs and the differential expression analysis. LMRGs were retrieved from four MSigDB gene sets, including Reactome data on the metabolism of lipids and lipoproteins, Reactome data on phospholipid metabolism, Hallmark data on fatty acid metabolism, and KEGG data on glycerophospholipid metabolism. Transcriptome data from OS patients and normal controls were obtained from the TARGET and GTEx databases. The differential expression analysis identified 176 DEGs among the LMRGs (Fig. 1A and B), indicating their potential involvement in the malignant progression of OS.

Subsequently, the expression data of the identified DEGs were obtained from the TARGET and GEO (GSE21257) databases to investigate the mechanisms of lipid metabolism in affecting OS development. UCR and MCR analyses were conducted to determine key risk factors. As detailed in Fig. 1C, the UCR analysis identified six significant genes ($p < 0.05$): *ALDH2*, *HSD17B3*, *SLC25A1*, *HSD17B8*, *SCD5*, and *HIBCH*. MCR analysis of these genes yielded a lipid metabolism-related prognostic RM (Fig. 1D–F). The RM was represented by the following formula: Risk score = (−0.261 × *ALDH2*) + (−1.937 × *HSD17B3*) + (−0.349 × *SLC25A1*) + (−0.469 × *HSD17B8*) + (−1.225 × *SCD5*) + 1.267 × *HIBCH*. Based on this formula, the prognostic risk value for each patient was computed, and patients were stratified into the HRG and LRG for subsequent analysis. The principal component analysis (PCA) was performed on 85 OS patients to preliminarily assess the performance of the prognostic RM. The findings revealed that patient stratification based on the RM values demonstrated more distinct group separation compared to clustering by the mean expression of all LMRGs.

3.2. Validation of the prognostic value of the lipid metabolism-related RM

The clinical significance of the prognostic RM for OS patients was further validated by evaluating its prognostic value. KM survival analysis unveiled that samples in the training (Fig. 2A) and validation datasets (Fig. 2B) were categorized into HRG and LRG based on the median risk score. The combined training and validation datasets were used to construct the prognostic RM, which was then substantiated through receiver operating characteristic (ROC) curve analysis. The area under the ROC curve (AUC) values for the RM and the 5YSR confirmed the predictive accuracy of the model for OS prognosis (Fig. 2C and D).

Risk scores for all patients with OS were calculated using the established risk formula. Based on these scores, patients were ranked and then categorized into the HRG and LRG according to the median risk score. The expression distribution of prognostic factors and patient survival status were visualized using a heatmap and a scatter plot (Fig. 2E). The nomogram (Fig. 2F) illustrates the prediction process for

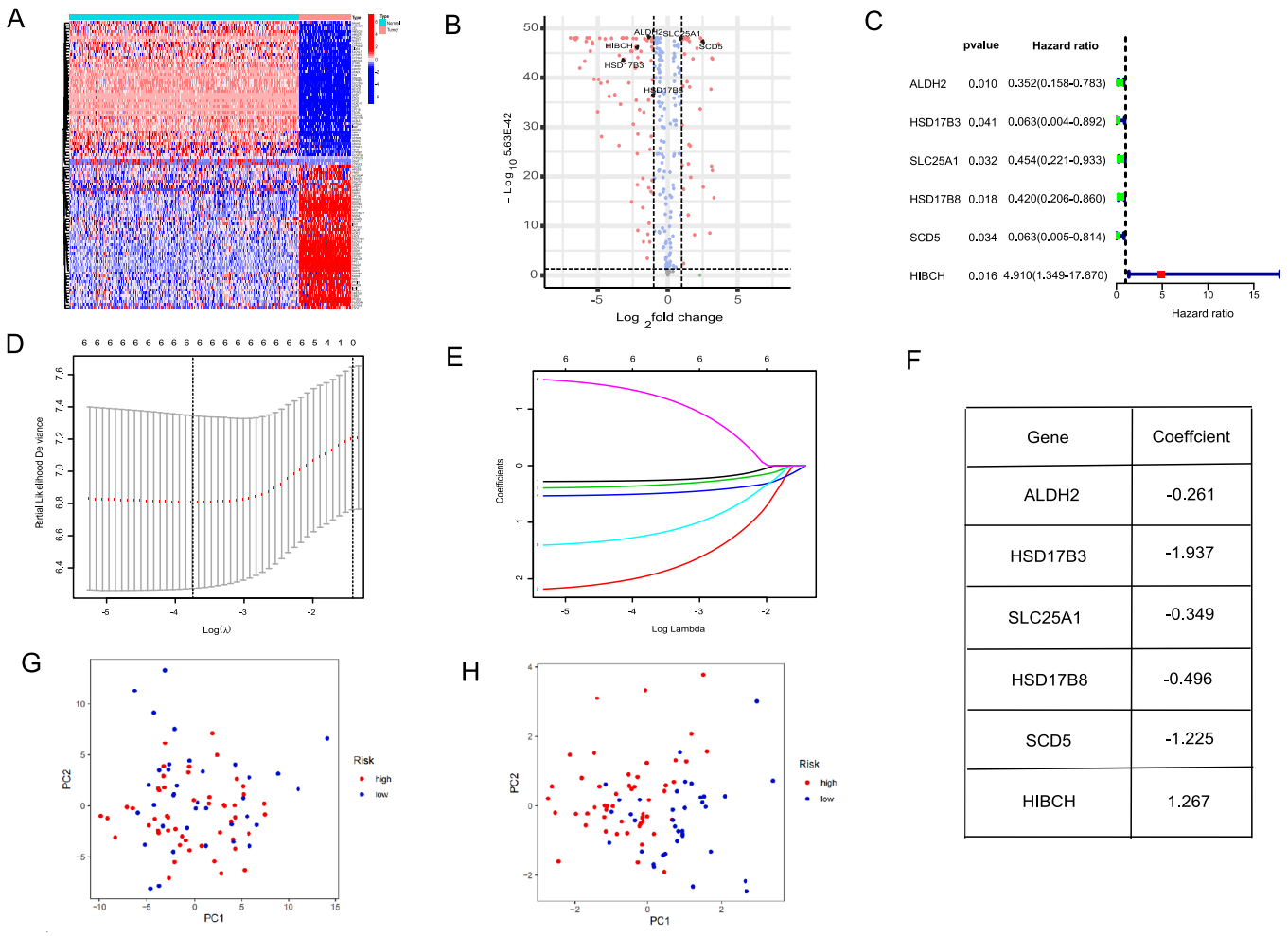

Gene	Coeffcient
ALDH2	-0.261
HSD17B3	-1.937
SLC25A1	-0.349
HSD17B8	-0.496
SCD5	-1.225
HIBCH	1.267

Fig. 1. Identification of LMRGs and development of a prognostic RM in OS. (A) Heatmap showing the expression patterns of 176 differentially expressed LMRGs between OS patients and normal controls. Data were obtained from the TARGET and GTEx databases. (B) Volcano plot illustrating the differential expression analysis results of LMRGs. Red dots represent upregulated genes, blue dots represent downregulated genes, and gray dots represent non-significantly changed genes. (C) Forest plot of UCR analysis results for the six significant LMRGs (*ALDH2*, *HSD17B3*, *SLC25A1*, *HSD17B8*, *SCD5*, and *HIBCH*) associated with OS prognosis ($p < 0.05$). (D) MCR analysis results for the six genes, showing their coefficients in the final RM. (E) KM survival curves comparing the HRG and LRG based on the developed RM in the training dataset. (F) Time-responsive ROC curves for the prognostic performance of the RM at different time points in the training dataset. (G) PCA plot comparing patient clustering based on the RM (left) versus clustering based on the mean expression of all LMRGs (right) in 85 patients with OS. OS, osteosarcoma; RM, risk model; LMRG, lipid metabolism-related gene; UCR, univariate Cox regression; MCR, multivariate Cox regression; HRG, high-risk group; LRG, low-risk group; KM, Kaplan-Meier; PCA, principal component analysis; HIBCH, 3-hydroxyisobutyryl-CoA hydrolase.

3-year survival rates (3YSRs) and 5YSRs in OS patients by combining the prognostic model scores with various clinical indicators for precise estimation.

The KM survival analysis was conducted for each gene included in the RM. In both training and validation datasets, only *HIBCH* exhibited a pronounced difference in overall survival between HRG and LRG ($p < 0.05$) (Supplementary Fig. 1). Consequently, further analysis was undertaken to explore the functional relevance of *HIBCH* in OS.

3.3. *HIBCH fosters proliferative capacity and clonogenic potential of OS cells*

The expression of HIBCH in OS cell lines and normal cells was initially assessed (Fig. 3A and B). HIBCH was found to be overexpressed in OS cell lines. Therefore, U2OS cells were selected for *HIBCH* knockdown experiments and U2R cells for *HIBCH* overexpression studies. The efficiency of knockdown and overexpression was corroborated by measuring HIBCH levels (Fig. 3C and D). Subsequent assays uncovered that *HIBCH* knockdown curbed the proliferative capacity and clonogenic potential of OS cells, whereas ectopic expression of *HIBCH* drove these biological processes (Fig. 3E and F).

3.4. *HIBCH upregulates migratory, invasive, and anti-apoptotic capabilities of OS cells*

Experiments were conducted to investigate the impacts of *HIBCH* on the migratory, invasive, and apoptotic capabilities of OS cells. The influence of *HIBCH* on epithelial-mesenchymal transition (EMT) was also examined due to the essential role of EMT in tumor cell migration and dissemination. *HIBCH* knockdown was found to constrain the migratory and invasive capacities of OS cells, while *HIBCH* overexpression facilitated the migratory and invasive capacities (Fig. 3G). Concurrently, *HIBCH* modulated the expression of EMT-related markers, including E-cadherin, N-cadherin, and vimentin (Fig. 3H). Flow cytometric detection revealed that, compared to the control group, *HIBCH* knockdown markedly expedited cell apoptosis and the expression of apoptosis-related factors cleaved-PARP and cleaved-CASP-9 in OS cells. In contrast, *HIBCH* overexpression diminished cell apoptosis (Fig. 3I and J). These results suggest that targeting *HIBCH* expression may offer a promising strategy to impede the malignant behaviors of OS cells.

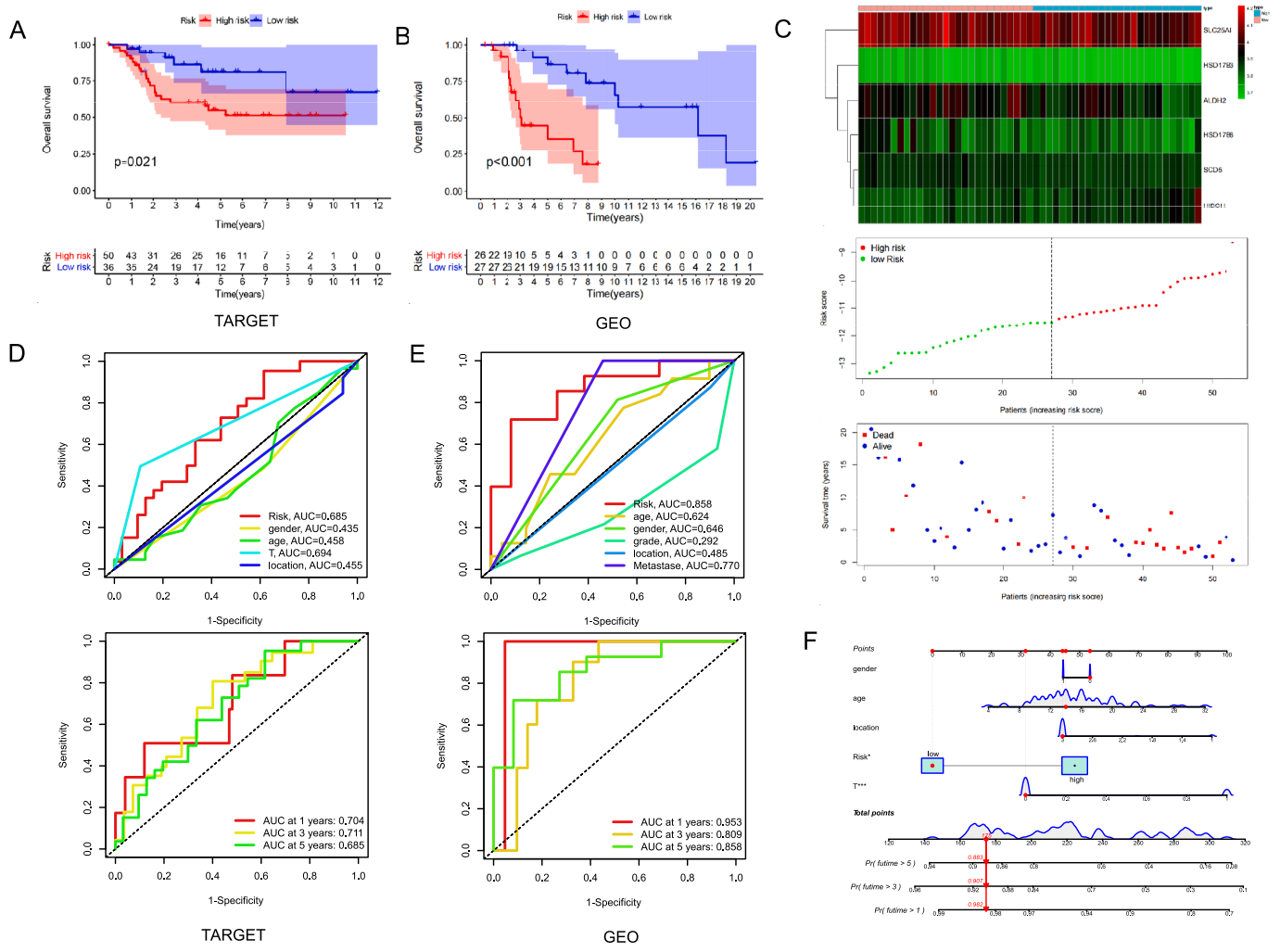

Fig. 2. Prognostic validation of the lipid metabolism-related RM in OS patients. (A) KM survival curves comparing the HRG and LRG based on the median risk score in the training dataset. (B) KM survival curves comparing the HRG and LRG based on the median risk score in the validation dataset. (C) ROC curve analysis of the RM for predicting overall survival in the combined training and validation datasets. (D) Time-responsive ROC curves for the prognostic performance of the RM for 5YSR. (E) Heatmap (top) showing the expression distribution of prognostic factors in the HRG and LRG. Scatter plot (bottom) displaying the distribution of patient survival status and risk scores. (F) Nomogram integrating the prognostic RM and various clinical indicators for predicting 3YSRs and 5YSRs in OS patients. OS, osteosarcoma; RM, risk model; LMRG, lipid metabolism-related gene; ROC, receiver operating characteristic; AUC, area under the ROC curve; 5YSR, 5-year survival rate; 3YSR, 3-year survival rate; HRG, high-risk group; LRG, low-risk group.

3.5. HIBCH knockdown curtails TCA cycle and oxidative phosphorylation (OXPHOS) in OS cells

The enzyme HIBCH, crucial in mitochondrial function and the valine degradation pathway, was analyzed to determine its metabolic effects on OS cells. The metabolic changes induced by *HIBCH* knockdown or overexpression were assessed using UFLC-MS, specifically targeting TCA cycle-related metabolites. The findings revealed that *HIBCH* knockdown markedly diminished the levels of oxaloacetate and succinate, key metabolites of succinyl-CoA in the TCA cycle (Fig. 4A). Conversely, *HIBCH* overexpression caused prominent increases in the metabolite levels (Fig. 4B). Furthermore, *HIBCH* overexpression escalated intracellular NADH levels (Fig. 4C), while siRNA-mediated *HIBCH* depletion led to pronounced reductions in NAD^+ and NADH levels (Fig. 4D). These observations suggest a role for *HIBCH* in lipid metabolism in OS cells through modulation of TCA cycle activity.

Previous research has delineated that SBF-1, a small molecule inhibitor, can inhibit HIBCH and thereby modulate cellular lipid metabolism [22]. Accordingly, OS cells were treated with HIBCH inhibitor SBF-1 to examine its effects on cell growth. The findings revealed that SBF-1 restricted the viability of OS cells (Fig. 4E and F). Further UFLC-MS analysis confirmed that SBF-1 treatment suppressed the TCA cycle activity, which was counteracted by *HIBCH* overexpression (Fig. 4G and H).

4. HIBCH inhibitor and DOX synergistically impede the malignant phenotypes of OS cells

The synergistic effects of CT agents were examined to explore the clinical potential of HIBCH inhibitors. It was indicated that the HIBCH inhibitor SBF-1 curtailed the viability of OS cells, and DOX, a commonly applied clinical CT agent for OS, repressed the viability of OS cells in a concentration-dependent manner (Fig. 5A). IC_{50} values of SBF-1 were determined for U2OS and U2R cell lines using CCK-8 assays after 48 h of treatment, yielding values of 46.12 nM and 38.14 nM, respectively. Correspondingly, the IC_{50} values for DOX were determined to be 231.14 nM for U2OS cells and 312.57 nM for U2R cells. The synergistic effects of SBF-1 and DOX were quantified in OS cell lines using the Chou-Talalay method. The data revealed that the combination of SBF-1 and DOX exhibited prominent synergistic cytotoxicity in U2OS and U2R cell lines, with CI values <1 (Fig. 5B). This finding signifies a pronounced synergistic effect in repressing OS cell viability. Hence, IC_{50} values of 120 nM

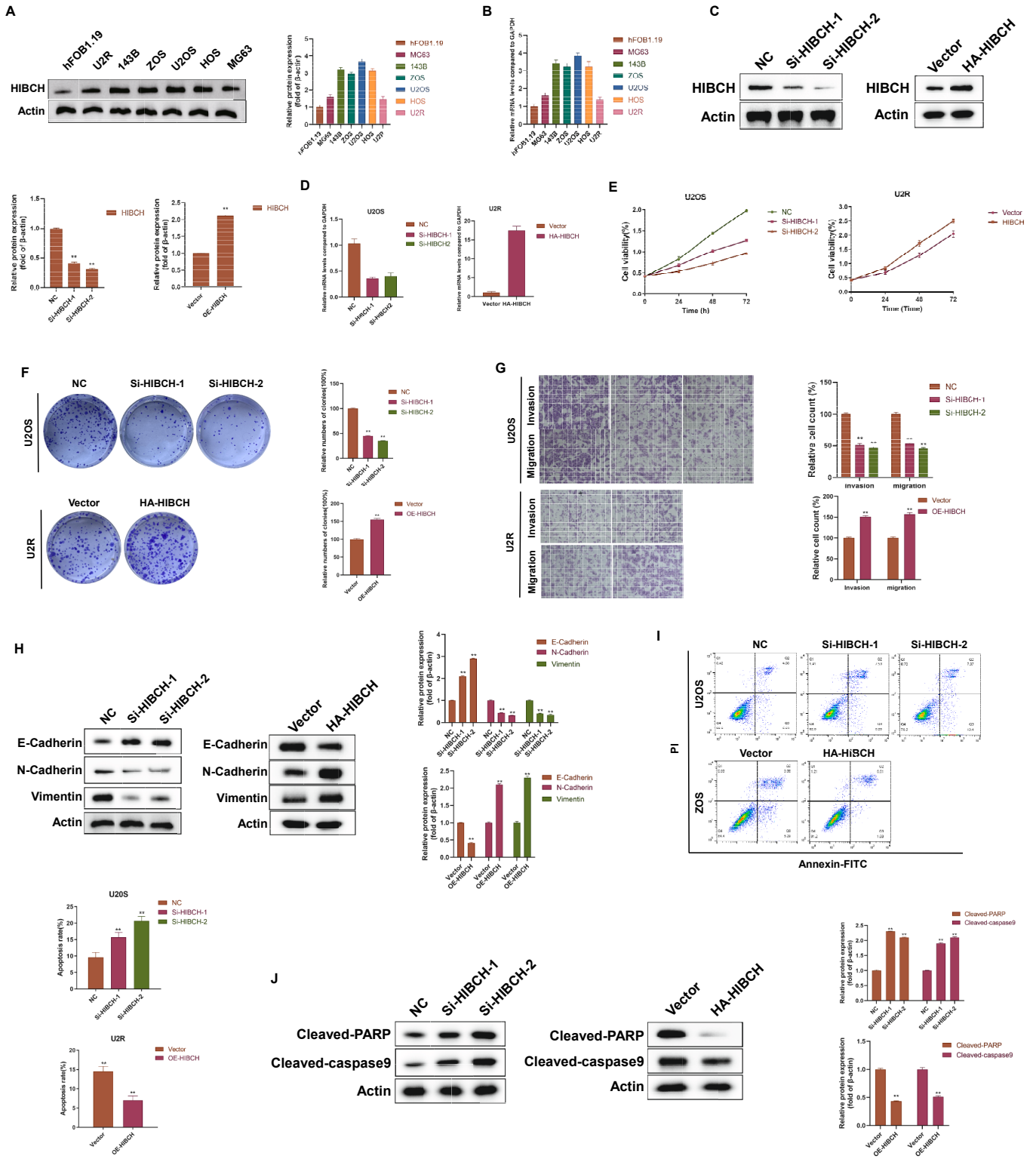

Fig. 3. *HIBCH* regulates proliferation, colony formation, and apoptosis of OS cells. (A and B) Western blots (A) and quantification (B) of HIBCH levels in OS cell lines and normal cells. (C and D) Verification of the efficiency of *HIBCH* knockdown in U2OS cells (C) and *HIBCH* overexpression in U2R cells (D) by Western blot assays. (E) Cell viability assay results of OS cells in response to *HIBCH* knockdown and overexpression compared to their respective controls. (F) Representative images and quantification of colony formation assays of OS cells in response to *HIBCH* knockdown and overexpression. (G) Transwell migration and invasion assay results of OS cells in response to *HIBCH* knockdown and overexpression. (H) Western blot analysis of EMT-related markers (E-cadherin, N-cadherin, and vimentin) of OS cells in response to *HIBCH* knockdown and overexpression. (I) Flow cytometric analysis of apoptosis of OS cells in response to *HIBCH* knockdown and overexpression compared to their respective controls. (J) Western blot analysis of apoptosis-related proteins (cleaved-PARP and cleaved-CASP-9) of OS cells in response to *HIBCH* knockdown and overexpression. Data are presented as mean ± SD from three independent experiments. $*p < 0.05$, $**p < 0.01$, $***p < 0.001$ compared to respective controls. OS, osteosarcoma; CASP-9, caspase-9; HIBCH, 3-hydroxyisobutyryl-CoA hydrolase.

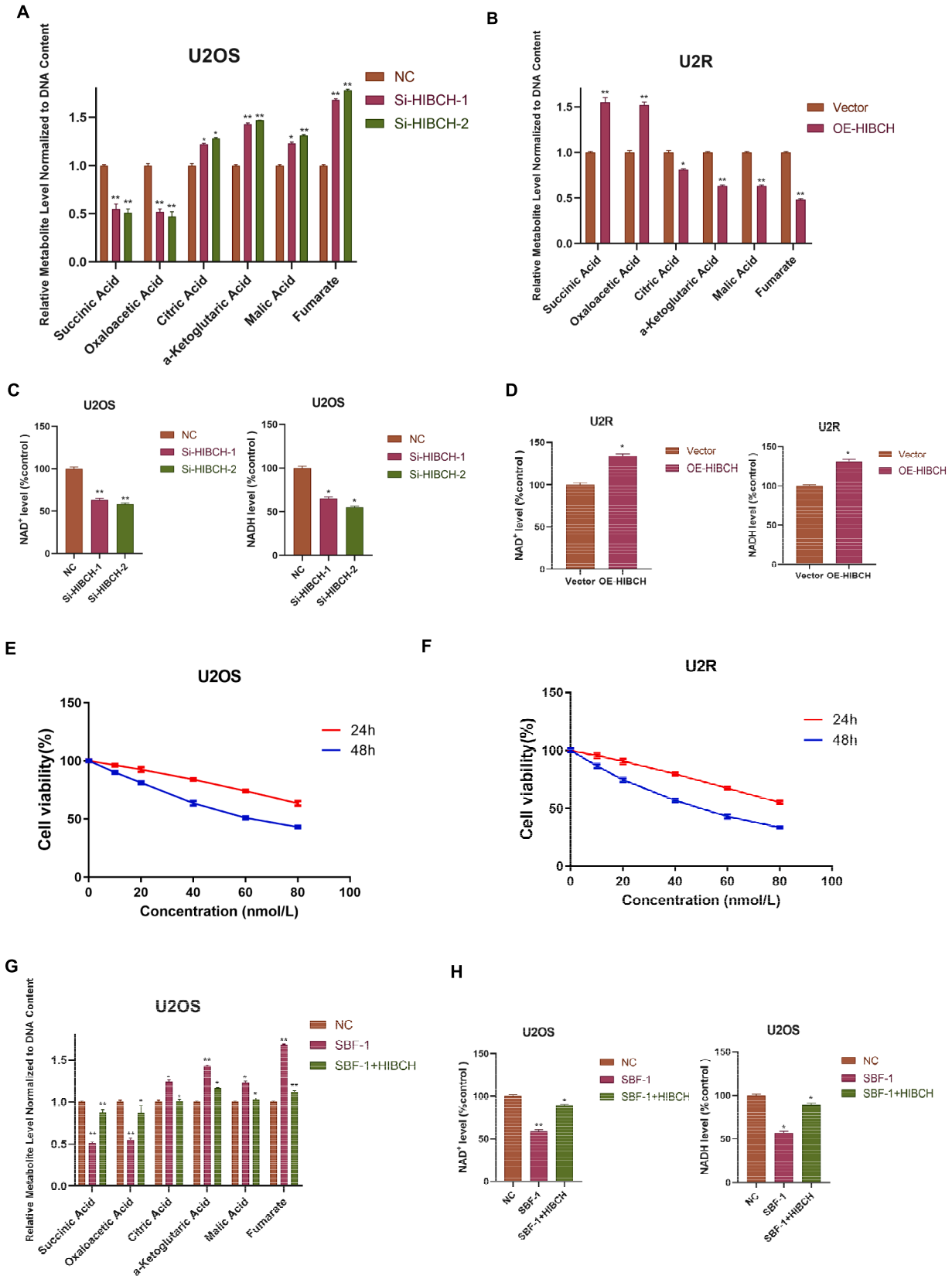

Fig. 4. *HIBCH* knockdown inhibits the TCA cycle and OXPHOS in OS cells. (A and B) Quantification of TCA cycle metabolites using UFLC-MS in U2OS or U2R cells with knockdown or overexpression of *HIBCH*. (C and D) Measurement of NAD^+ (left) and NADH (right) levels using EnVision multimode plate reader in U2OS or U2R cells with knockdown or overexpression of *HIBCH*. (E and F) Assessment of cell viability using CCK-8 assay in U2OS and U2R cells treated with varying concentrations of HIBCH inhibitor SBF-1 for 24 and 48 h. (G and H) Quantification of TCA cycle metabolites using UFLC-MS in U2OS or U2R cells under indicated treatments. OS, osteosarcoma; TCA, tricarboxylic acid; OXPHOS, oxidative phosphorylation; HIBCH, 3-hydroxyisobutyryl-CoA hydrolase.

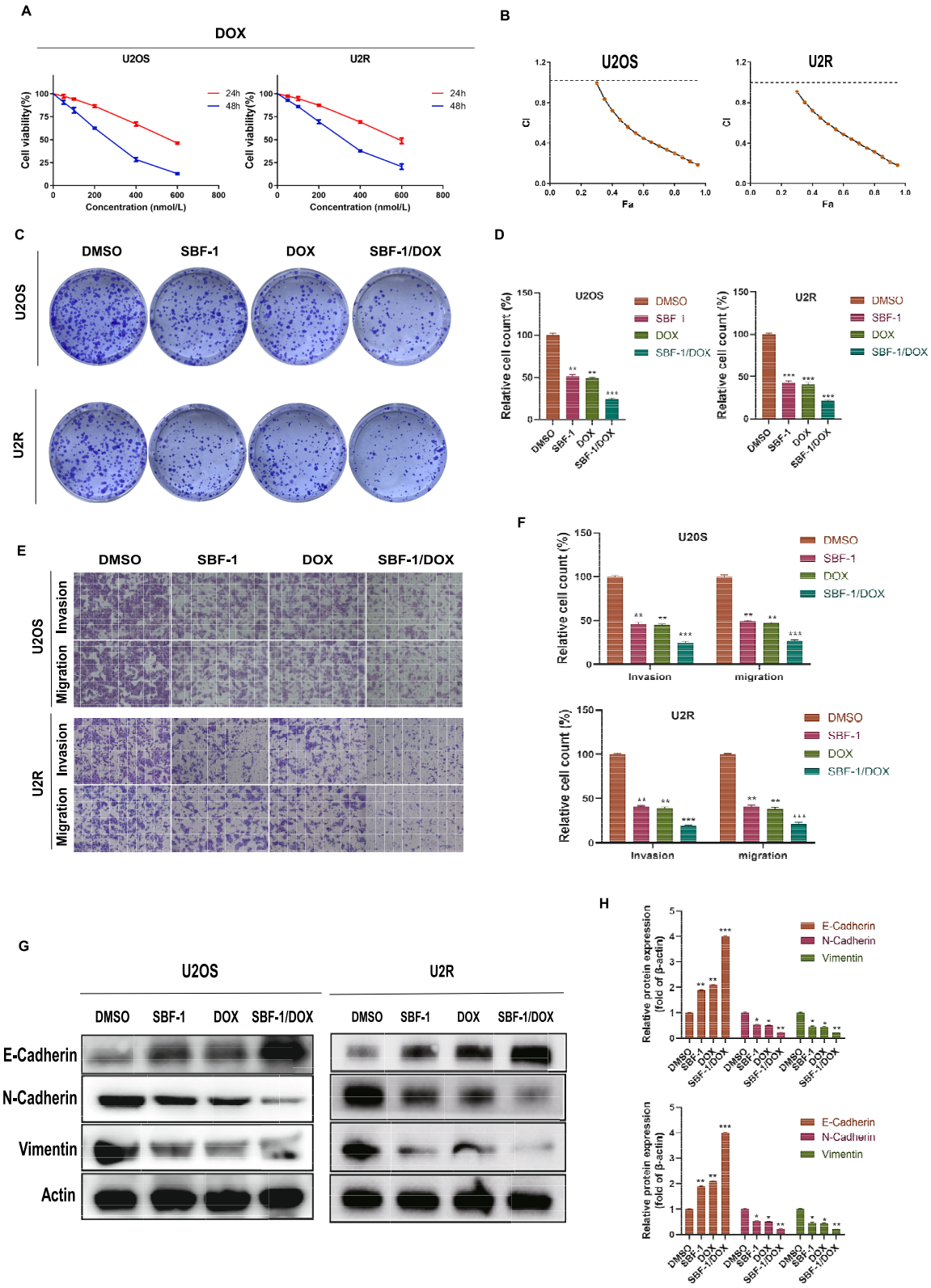

Fig. 5. Synergistic effects of HIBCH inhibitor SBF-1 and DOX on OS cells. (A) Dose-responsive curves of SBF-1 and DOX in U2OS and U2R cells after 48 h of treatment. IC_{50} values are indicated. (B) CI plots for SBF-1 and DOX in U2OS and U2R cells, as computed using the Chou-Talalay method. CI < 1 indicates synergism. (C and D) Representative images (C) and quantification (D) of colony formation assays in U2OS and U2R cells treated as indicated. (E and F) Representative images (E) and quantification (F) of Transwell migration and invasion assays in U2OS and U2R cells treated as indicated. (G and H) Western blots (G) and densitometric quantification (H) of the levels of EMT-related markers (E-cadherin, N-cadherin, and vimentin) in U2OS and U2R cells treated as indicated. Cells were treated with DMSO (control), SBF-1 (40 nM), DOX (120 nM), or their combination for 48 h in all experiments unless otherwise stated. Data in panels D, F, and H are presented as mean ± SD from three independent experiments. *$p < 0.05$, **$p < 0.01$, ***$p < 0.001$ compared to control. OS, osteosarcoma; DOX, doxorubicin; CI, combination index; HIBCH, 3-hydroxyisobutyryl-CoA hydrolase.

for DOX and 40 nM for SBF-1 were selected for subsequent combination treatment experiments.

The effects of combination treatment on the oncogenic behaviors of OS cells were further examined. Cells were treated with control (DMSO), SBF-1 (40 nM) alone, DOX (120 nM) alone, or a combination of both agents for 48 h. Colony formation and Transwell assays suggested that compared to single-agent treatments, the combination treatment markedly bolstered the inhibition of clonogenic potential (Fig. 5C and D) and the migratory and invasive capabilities (Fig. 5E and F) of OS cells. Western blot analysis confirmed these findings by showing a reduction in vimentin and N-cadherin levels and an upregulation in E-cadherin levels in the combination treatment group (Fig. 5G and H). These data imply that the combination treatment may diminish the invasion of OS cells by modulating EMT. Flow cytometric detection further demonstrated that the simultaneous administration of SBF-1 and DOX markedly elevated apoptosis rates of OS cells, substantially exceeding the levels observed in single-agent treatments (Fig. 6A and B). This effect was accompanied by a notable upregulation of the activated forms of apoptosis-related proteins PARP and CASP-9 in the combination treatment group (Fig. 6C and D). Given the established role of the Akt-mTOR pathway in regulating lipid metabolism in OS [22], the involvement of this pathway was assessed in our study. The results demonstrated that SBF-1 and DOX synergistically repressed the malignant phenotypes of OS cells through the Akt-mTOR pathway (Fig. 6E and F), thus contributing to a deeper understanding of the involvement of the Akt-mTOR pathway in lipid metabolism regulation in OS.

4.1. SBF-1 and DOX synergistically enhance the anti-OS effects in vivo

To further substantiate the *in vitro* findings, an immunodeficient mouse model with OS cell xenograft was used to evaluate the anti-OS effects of SBF-1 and DOX alone or in combination. Accordingly, SBF-1 or DOX alone prominently attenuated the tumor growth of OS cell-bearing mice. Notably, the combination of these two agents exhibited

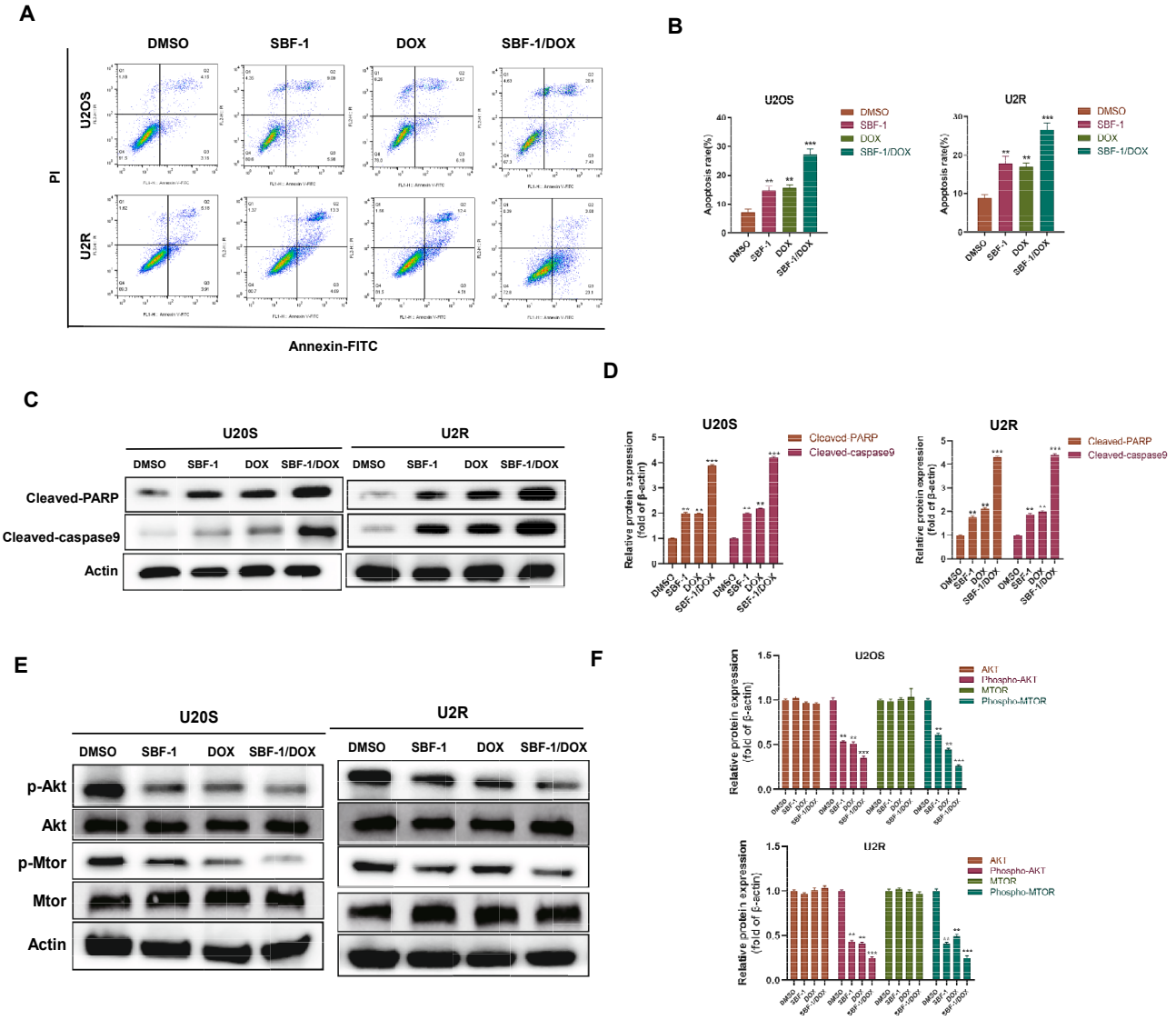

Fig. 6. Combination of SBF-1 and DOX enhances apoptosis and inhibits the Akt-mTOR pathway in OS cells. Flow cytometry plots showing apoptosis of U2OS and U2R cells treated as indicated. (B) Quantification of apoptosis rates from (A). (C) Western blot analysis of apoptosis-related proteins (cleaved PARP and cleaved CASP-9) in U2OS and U2R cells treated as indicated. (D) Densitometric quantification of protein levels from (C), as normalized to β-actin. (E) Western blot analysis of Akt-mTOR pathway-related proteins (p-Akt, Akt, p-mTOR, mTOR) in U2OS and U2R cells treated as indicated. (F) Densitometric quantification of protein levels from (E), as normalized to total protein levels or β-actin as appropriate. Data in panels B, D, and F are presented as mean ± SD from three independent experiments. Cells were treated with DMSO (control), SBF-1 (40 nM), DOX (120 nM), or their combination for 48 h in all experiments. $*p < 0.05$, $**p < 0.01$, $***p < 0.001$ compared to control. OS, osteosarcoma; DOX, doxorubicin; CASP-9, caspase-9.

more robust synergistic inhibitory impacts (Fig. 7A–C). The *in vivo* experiments provided evidence supporting the synergistic action of SBF-1 and DOX in suppressing OS growth.

5. Discussion

Despite considerable progress in OS treatment in recent decades, the long-term survival rate for patients with OS remains disappointingly low [1,2]. Conventional treatment modalities, such as surgery, radiotherapy, and CT, while effective in some scenarios, offer limited options for patients with advanced or recurrent OS and often result in severe adverse effects [24]. This context underscores the necessity for developing novel therapeutic strategies, particularly molecule-targeted therapies, to enhance the survival outcomes and quality of life for OS patients.

In this study, an RM based on LMRGs was developed to predict the malignancy of OS. The analysis identified a prognostic RM comprising six key genes (*ALDH2*, *HSD17B3*, *SLC25A1*, *HSD17B8*, *SCD5*, and *HIBCH*). This study specifically highlighted the functional role of *HIBCH* in OS progression. Experimental data demonstrated that *HIBCH* fostered the proliferative, migratory, invasive, and anti-apoptotic capabilities of OS cells. Further mechanistic studies elucidated that *HIBCH* modulated the lipid metabolism of OS cells by regulating the TCA cycle and OXPHOS.

The significance of lipid metabolism in OS has recently garnered widespread interest. Prior research has established that lipid metabolism disturbances are robustly associated with the carcinogenic mechanism and prognostic outcomes in the context of OS [25]. For instance, the long non-coding RNA RPARP-AS1 has been shown to escalate the proliferative capacity of OS cells by modulating lipid metabolism [26]. Specifically, RPARP-AS1 upregulates key lipogenic enzymes and potentially drives lipid metabolism in OS cells *via* regulation of the Akt-mTOR pathway [26]. Furthermore, the interplay between cellular autophagy and lipid metabolism in OS cells presents intricate connections [27]. Under stress conditions, autophagy in OS cells is modulated through various cellular signaling cascades, and alterations in lipid metabolism play a vital role in maintaining endoplasmic reticulum homeostasis and supporting autophagic functions [28]. Recent research using 3D-printed composite scaffold-based OS models has further elucidated the pathogenesis of OS and highlighted substantial variations in lipid metabolism, thereby providing promising insights for new diagnostic and therapeutic approaches [28].

This preliminary study contributes to the understanding of LMRGs in OS and uncovers their involvement in tumor malignant transformation and CT resistance. The findings underscore the critical role of lipid metabolism in supporting the energy supply and biosynthetic processes of OS cells and propose its potential regulation of key biological processes, such as cell signaling, cell cycle entry, and apoptotic potential. These insights open new avenues for therapeutic development and may offer potential strategies to enhance OS patient outcomes. However, further investigation is warranted to fully assess the clinical relevance and application of these insights.

A notable finding from this study is the dose-responsive inhibition of OS by the HIBCH inhibitor SBF-1, along with evidence of its synergistic effects when combined with DOX. Since the 1970s, CT has been a cornerstone of OS treatment and markedly facilitates patient survival rates [29–31]. Currently, the standard treatment for OS integrates surgery with neoadjuvant CT, with conventional CT regimens incorporating agents such as cisplatin, DOX, methotrexate, and ifosfamide [4,32–35]. Despite advancements in CT efficacy, the clinical prognosis of OS remains dismal. Approximately one-third of OS patients demonstrate poor responses to CT agents, often resulting in recurrence and metastasis and 5YSRs as low as 5–20 % [1,2,36–38]. CT resistance is a formidable challenge in OS treatment [38]. The emergence of CT resistance curtails the effectiveness of CT and raises the risk of treatment failure. For instance, the upregulation of multidrug resistance genes has been shown to accelerate the resistance of tumor cells to multiple CT agents, further complicating treatment outcomes [39].

Our study revealed the synergistic effect between HIBCH inhibitor SBF-1 and DOX and offered promising implications for OS treatment. SBF-1, a small molecule inhibitor, has been noted for its capacity to modulate cellular lipid metabolism. The obtained data delineated that SBF-1 prominently suppressed the malignant phenotypes of OS cells and, when combined with DOX, led to substantial synergistic cytotoxic effects. The combination of SBF-1 with DOX could enhance the effectiveness of CT while potentially reducing the development of resistance. This study reinforces the essential role of CT in OS treatment and highlights the potential of novel drug combinations to address resistance challenges. Future research should further explore the mechanisms of this synergistic action and evaluate its translational potential for clinical applications.

This study highlights the role of *HIBCH* in the development of OS and introduces a novel therapeutic strategy based on HIBCH inhibition. Nevertheless, several limitations suggest avenues for further research. First, the lipid metabolism-related RM presented in this study was developed using a relatively small patient cohort. While its prognostic value was validated in training and validation datasets, broadening the sample size to include more diverse OS cases across different subtypes and stages would reinforce its validation and clinical applicability. Additionally, the specific molecular mechanisms by which *HIBCH* regulates OS cell metabolism and malignant phenotypes are not fully delineated. For example, the interactions between HIBCH and other metabolic regulators affecting the TCA cycle and OXPHOS remain to be

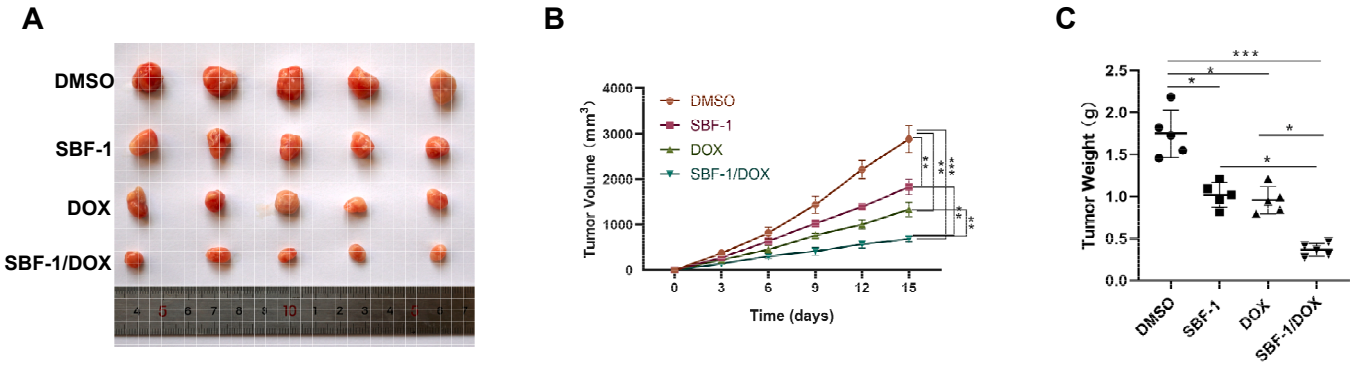

Fig. 7. SBF-1 and DOX synergistically inhibit OS cell xenograft growth *in vivo*. (A) Changes in tumor volumes over time in immunodeficient mice bearing OS cell xenografts treated with control (DMSO), SBF-1 alone, DOX alone, or their combination. (B) Tumor weights at the endpoint of the experiment for each treatment group. (C) Tumor growth inhibition rates for SBF-1, DOX, and their combination, computed as the percentage reduction in tumor volume compared to the control group. OS, osteosarcoma; DOX, doxorubicin.

clarified. Future studies should delve into the detailed mechanisms underlying HIBCH-mediated metabolic reprogramming to reveal novel therapeutic targets. Although preclinical data on the combination of HIBCH inhibitor SBF-1 with DOX are encouraging, significant challenges remain in translating these results to clinical settings. Comprehensive assessments of drug safety and dosage optimization studies are needed in future studies. Moreover, the potential for combining HIBCH inhibitors with other CT or targeted drugs should be explored to expand therapeutic options.

In conclusion, this study elucidates the promising role of lipid metabolism in OS progression and proposes a novel therapeutic strategy involving HIBCH inhibition. A lipid metabolism-related RM was developed to predict the malignancy of OS, and *HIBCH* was pinpointed as a key factor in OS development. The study indicated that *HIBCH* fostered the proliferative, migratory, invasive, and anti-apoptotic capabilities of OS cells by regulating the TCA cycle and OXPHOS. Importantly, the HIBCH inhibitor SBF-1 exhibited synergistic effects with DOX in curbing OS growth both in *in vitro* experiments and animal models. This combination treatment demonstrated more potent effects in diminishing malignant phenotypes of OS cells, when compared to single-agent treatment. The findings offer an initial insight into the involvement of lipid metabolism in OS and indicate promising avenues to suppress CT resistance. This study underlines the need for extensive future studies to elucidate the underlying molecular mechanisms and assess their translational potential for clinical strategies.

CRediT authorship contribution statement

Xuhui Yuan: Writing – original draft, Visualization, Validation, Software, Methodology. **Bo Yu:** Writing – original draft, Visualization, Methodology. **Haiqi Ding:** Investigation, Formal analysis, Conceptualization. **Hongyan Li:** Investigation, Formal analysis, Conceptualization. **Qijing Wang:** Investigation, Formal analysis, Conceptualization. **Lan Lin:** Investigation, Formal analysis, Conceptualization. **Wenming Zhang:** Writing – review & editing, Supervision, Resources. **Xinyu Fang:** Writing – review & editing, Resources, Project administration, Methodology.

Declaration of competing interest

The authors declare that they have no known competing financial interests or personal relationships that could have appeared to influence the work reported in this paper.

Acknowledgements

We express our sincere gratitude to the TARGET database, GTEx database, and GEO database for their invaluable resources and support.

Funding

This work was supported by the National Natural Science Foundation of China (Grant number: 82371375), the Fujian Medical Innovation Grant, China (Grant number: 2023CXA020), the Fujian Research and Training Grants for Young and Middle-aged Leaders in Healthcare (Grant number: 2023ZQNRCYX-FXY).

Author contributions

Xuhui Yuan and Bo Yu contributed equally to this work as co-first authors. Xuhui Yuan conceived the study, designed the experiments, and wrote the initial draft of the manuscript. Bo Yu performed data analysis, interpreted the results, and contributed to manuscript writing. Haiqi Ding and Hongyan Li conducted experimental work and assisted with data collection. Qijin Wang provided technical support and contributed to methodology development. Lan Lin assisted with data interpretation and manuscript revision. Wenming Zhang and Xinyu Fang share corresponding authorship. They supervised the project, provided critical feedback, and were responsible for the final approval of the manuscript. All authors reviewed and agreed to the published version of the manuscript.

Ethics and consent to participate

All animal care and experiments in this study were approved by the Ethics Committee of Fujian Medical University (FJMU IACUC 2020-0013), and the study was reported according to the ARRIVE guidelines. The transcriptome data pertaining to patients used in this research were obtained from three publicly accessible databases: TARGET, GTEx, and GEO. Owing to the public availability of these datasets, no supplementary ethical clearance was necessitated.

Appendix A. Supplementary data

Supplementary data to this article can be found online at https://doi.org/10.1016/j.jbo.2024.100652.

Data availability

The data supporting the findings of this study are available upon request from the corresponding author. For further resources, the TARGET database (https://ocg.cancer.gov/programs/target), in conjunction with the GEO database (http://www.ncbi.nlm.nih.gov/geo/) and the GTEx database (https://www.gtexportal.org/home/), provide access to the datasets used in this research.

References

[1] S. Cole, D.M. Gianferante, B. Zhu, et al., Osteosarcoma: a surveillance, epidemiology, and end results program-based analysis from 1975 to 2017, Cancer 128 (11) (2022) 2107–2118, https://doi.org/10.1002/cncr.34163.
[2] L. Mirabello, R.J. Troisi, S.A. Savage, Osteosarcoma incidence and survival rates from 1973 to 2004: data from the Surveillance, Epidemiology, and End Results Program, Cancer: Interdiscip. Int. J. Am. Cancer Soc. 115 (7) (2009) 1531–1543, https://doi.org/10.1002/cncr.24121.
[3] P.C. Valery, M. Laversanne, F. Bray, Bone cancer incidence by morphological subtype: a global assessment, Cancer Causes Control 26 (2015) 1127–1139, https://doi.org/10.1007/s10552-015-0607-3.
[4] D.D. Moore, H.H. Luu, Osteosarcoma, Orthopaedic Oncol. (2014) 65–92, https://doi.org/10.1007/978-3-319-07323-1_4.
[5] D.M. Gianferante, L. Mirabello, S.A. Savage, Germline and somatic genetics of osteosarcoma—connecting aetiology, biology and therapy, Nat. Rev. Endocrinol. 13 (8) (2017) 480–491, https://doi.org/10.1038/nrendo.2017.16.
[6] C.R. Bartman, B. Faubert, J.D. Rabinowitz, et al., Metabolic pathway analysis using stable isotopes in patients with cancer, Nat. Rev. Cancer 23 (12) (2023) 863–878, https://doi.org/10.1038/s41568-023-00632-z.
[7] T. Ge, X. Gu, R. Jia, et al., Crosstalk between metabolic reprogramming and epigenetics in cancer: updates on mechanisms and therapeutic opportunities, Cancer Commun. 42 (11) (2022) 1049–1082, https://doi.org/10.1002/cac2.12374.
[8] L. Xia, L. Oyang, J. Lin, S. Tan, Y. Han, N. Wu, P. Yi, L. Tang, Q. Pan, S. Rao, J. Liang, Y. Tang, M. Su, X. Luo, Y. Yang, Y. Shi, H. Wang, Y. Zhou, Q. Liao, The cancer metabolic reprogramming and immune response, Mol. Cancer 20 (2021) 28, https://doi.org/10.1186/s12943-021-01316-8.
[9] K. Yang, X. Wang, C. Song, et al., The role of lipid metabolic reprogramming in tumor microenvironment, Theranostics 13 (6) (2023) 1774, https://doi.org/10.7150/thno.82920.
[10] C. Cheng, F. Geng, X. Cheng, D. Guo, Lipid metabolism reprogramming and its potential targets in cancer, Cancer Commun. 38 (2018) 27, https://doi.org/10.1186/s40880-018-0301-4.
[11] A. Khan, S. Siddiqui, S.A. Husain, et al., Phytocompounds targeting metabolic reprogramming in cancer: an assessment of role, mechanisms, pathways, and therapeutic relevance, J. Agric. Food Chem. 69 (25) (2021) 6897–6928, https://doi.org/10.1021/acs.jafc.1c01173.
[12] Y. Cao, Adipocyte and lipid metabolism in cancer drug resistance, J. Clin. Invest. 129 (8) (2019) 3006–3017, https://doi.org/10.1172/JCI127201.
[13] Z. Gong, Q. Li, J. Shi, et al., Lipid-laden lung mesenchymal cells foster breast cancer metastasis via metabolic reprogramming of tumor cells and natural killer cells, Cell Metab. 34 (12) (2022), https://doi.org/10.1016/j.cmet.2022.11.003, pp. 1960–1976. e9.
[14] D. Zipinotti dos Santos, J.C. de Souza, T.M. Pimenta, et al., The impact of lipid metabolism on breast cancer: a review about its role in tumorigenesis and immune

escape, Cell Commun. Signal. 21 (1) (2023) 161, https://doi.org/10.1186/s12964-023-01178-1.
[15] Z. Zhang, W. Wang, P. Kong, et al., New insights into lipid metabolism and prostate cancer, Int. J. Oncol. 62 (6) (2023) 1–13, https://doi.org/10.3892/ijo.2023.5522.
[16] W. Dai, W. Xiang, L. Han, et al., PTPRO represses colorectal cancer tumorigenesis and progression by reprogramming fatty acid metabolism, Cancer Commun. 42 (9) (2022) 848–867, https://doi.org/10.1002/cac2.12341.
[17] X. Sun, C. Shi, J. Dai, M.Q. Zhang, D.S. Pei, L. Yang, Targeting the mitochondrial protein YME1L to inhibit osteosarcoma cell growth in vitro and in vivo, Cell Death Dis. 15 (2024) 346, https://doi.org/10.1038/s41419-024-06722-6.
[18] Y. Shi, S. Wu, X. Zhang, et al., Lipid metabolism-derived FAAH is a sensitive marker for the prognosis and immunotherapy of osteosarcoma patients, Heliyon 10 (1) (2024), https://doi.org/10.1016/j.heliyon.2023.e23499.
[19] S. Lin, Y. Miao, X. Zheng, et al., ANGPTL4 negatively regulates the progression of osteosarcoma by remodeling branched-chain amino acid metabolism, Cell Death Discov. 8 (1) (2022) 225, https://doi.org/10.1038/s41420-022-01029-x.
[20] Y. Pan, J. Yang, Y. Gong, et al., 3-Hydroxyisobutyryl-CoA hydrolase involved in isoleucine catabolism regulates triacylglycerol accumulation in Phaeodactylum tricornutum, Philos. Trans. R. Soc. B 372 (1728) (2017) 20160409, https://doi.org/10.1098/rstb.2016.0409.
[21] L. Yang, X. Wang, J. Liu, et al., Prognostic and tumor microenvironmental feature of clear cell renal cell carcinoma revealed by m6A and lactylation modification-related genes, Front. Immunol. 14 (2023) 1225023, https://doi.org/10.3389/fimmu.2023.1225023.
[22] Y. Shan, Y. Gao, W. Jin, et al., Targeting HIBCH to reprogram valine metabolism for the treatment of colorectal cancer, Cell Death Dis. 10 (8) (2019) 618, https://doi.org/10.1038/s41419-019-1832-6.
[23] J.N. Graff, S. Puri, C.B. Bifulco, et al., Sustained complete response to CTLA-4 blockade in a patient with metastatic, castration-resistant prostate cancer, Cancer Immunol. Res. 2 (5) (2014) 399–403, https://doi.org/10.1158/2326-6066.CIR-13-0193.
[24] R. Belayneh, M.S. Fourman, S. Bhogal, et al., Update on osteosarcoma, Curr. Oncol. Rep. 23 (2021) 1–8, https://doi.org/10.1007/s11912-021-01053-7.
[25] H. Qian, T. Lei, Y. Hu, et al., Expression of lipid-metabolism genes is correlated with immune microenvironment and predicts prognosis in osteosarcoma, Front. Cell Dev. Biol. 9 (2021) 673827, https://doi.org/10.3389/fcell.2021.673827.
[26] F. Cai, L. Liu, Y. Bo, et al., LncRNA RPARP-AS1 promotes the progression of osteosarcoma cells through regulating lipid metabolism, BMC Cancer 24 (1) (2024) 166, https://doi.org/10.1186/s12885-024-11901-x.
[27] Y. Ogasawara, J. Cheng, T. Tatematsu, et al., Long-term autophagy is sustained by activation of CCTβ3 on lipid droplets, Nat. Commun. 11 (1) (2020) 4480, https://doi.org/10.1038/s41467-020-18153-w.
[28] N. Leitner, J. Hlavatý, R. Ertl, et al., Lipid droplets and perilipins in canine osteosarcoma. Investigations on tumor tissue, 2D and 3D cell culture models, Vet. Res. Commun. 46 (4) (2022) 1175–1193, https://doi.org/10.1007/s11259-022-09975-8.
[29] N. Jaffe, Recent advances in the chemotherapy of metastatic osteogenic sarcoma, Cancer 30 (6) (1972) 1627–1631, https://doi.org/10.1002/1097-0142(197212)30:6<1627::aid-cncr2820300631>3.0.co;2-h.
[30] G. Rosen, Neoadjuvant chemotherapy for osteogenic sarcoma: a model for the treatment of other highly malignant neoplasms, in: Preoperative (Neoadjuvant) Chemotherapy, Springer Berlin Heidelberg, Berlin, Heidelberg, 1986, pp. 148–157. doi:10.1007/978-3-642-82671-9_17.
[31] Y. Zhang, J. Yang, N. Zhao, et al., Progress in the chemotherapeutic treatment of osteosarcoma, Oncol. Lett. 16 (5) (2018) 6228–6237, https://doi.org/10.3892/ol.2018.9434.
[32] W.Q. Wu, C.D. Zou, D. Wu, et al., Construction of molecular subtype model of osteosarcoma based on endoplasmic reticulum stress and tumor metastasis-related genes, Heliyon 10 (3) (2024), https://doi.org/10.1093/annonc/mdq276.
[33] Y. Chen, R. Liu, W. Wang, et al., Advances in targeted therapy for osteosarcoma based on molecular classification, Pharmacol. Res. 169 (2021) 105684, https://doi.org/10.1016/j.phrs.202 1.105684.
[34] D. Carrle, S.S. Bielack, Current strategies of chemotherapy in osteosarcoma, Int. Orthopaedics 30 (2006) 445–451, https://doi.org/10.1007/s00264-006-0192-x.
[35] J.C. Wittig, J. Bickels, D. Priebat, et al., Osteosarcoma: a multidisciplinary approach to diagnosis and treatment, Am. Fam. Physician 65 (6) (2002) 1123–1133.
[36] M. Sampo, M. Koivikko, M. Taskinen, et al., Incidence, epidemiology and treatment results of osteosarcoma in Finland–a nationwide population-based study, Acta Oncol. 50 (8) (2011) 1206–1214, https://doi.org/10.3109/0284186X.2011.615339.
[37] J.A. Lee, J. Lim, H.Y. Jin, et al., Osteosarcoma in adolescents and young adults, Cells 10 (10) (2021) 2684, https://doi.org/10.3390/cells10102684.
[38] P. Fu, Y. Shi, G. Chen, et al., Prognostic factors in patients with osteosarcoma with the surveillance, epidemiology, and end results database, Technol. Cancer Res. Treat. 19 (2020) 1533033820947701, https://doi.org/10.1177/1533033820947701.
[39] J.Z. Yang, S.R. Ma, X.L. Rong, et al., Characterization of multidrug–resistant osteosarcoma sublines and the molecular mechanisms of resistance, Mol. Med. Rep. 14 (4) (2016) 3269–3276, https://doi.org/10.3892/mmr.2016.5590.